Shape change in the receptor for gliding motility in *Plasmodium* sporozoites

Gaojie Song, Adem C. Koksal, Chafen Lu, and Timothy A. Springer[1]

Immune Disease Institute, Program in Cellular and Molecular Medicine, Children's Hospital Boston, MA 02115; and Department of Biological Chemistry and Molecular Pharmacology, Harvard Medical School, Boston, MA 02115

Contributed by Timothy A. Springer, October 29, 2012 (sent for review October 11, 2012)

Sporozoite gliding motility and invasion of mosquito and vertebrate host cells in malaria is mediated by thrombospondin repeat anonymous protein (TRAP). Tandem von Willebrand factor A (VWA) and thrombospondin type I repeat (TSR) domains in TRAP connect through proline-rich stalk, transmembrane, and cytoplasmic domains to the parasite actin-dependent motility apparatus. We crystallized fragments containing the VWA and TSR domains from *Plasmodium vivax* and *Plasmodium falciparum* in different crystal lattices. TRAP VWA domains adopt closed and open conformations, and bind a Mg^{2+} ion at a metal ion–dependent adhesion site implicated in ligand binding. Metal ion coordination in the open state is identical to that seen in the open high-affinity state of integrin I domains. The closed VWA conformation associates with a disordered TSR domain. In contrast, the open VWA conformation crystallizes with an extensible β ribbon and ordered TSR domain. The extensible β ribbon is composed of disulfide-bonded segments N- and C-terminal to the VWA domain that are largely drawn out of the closed VWA domain in a 15 Å movement to the open conformation. The extensible β ribbon and TSR domain overlap at a conserved interface. The VWA, extensible β ribbon, and TSR domains adopt a highly elongated overall orientation that would be stabilized by tensile force exerted across a ligand-receptor complex by the actin motility apparatus of the sporozoite. Our results provide insights into regulation of "stick-and-slip" parasite motility and for development of sporozoite subunit vaccines.

Mosquitoes transmit malaria to humans via sporozoites. Sporozoites are important targets of pre-erythrocytic malaria vaccines. However, we know little about the structure and arrangement of the two most important vaccine targets on sporozoite surfaces, the circumsporozoite (CS) protein (1–3) and thrombospondin repeat anonymous protein (TRAP) (4, 5). CS is a constitutive sporozoite surface protein and has a glycophosphatidylinositol anchor. TRAP mediates sporozoite gliding motility and cell invasion in both mosquito and vertebrate hosts (6).

TRAP is mobilized from micronemes to the plasma membrane at the apical end of sporozoites, and is translocated to the posterior end during cell migration and invasion (7, 8). TRAP spans the plasma membrane, and its cytoplasmic domain connects to the actin cytoskeleton through aldolase, permitting functional cooperation between extracellular adhesive domains and the intracellular actin/myosin motor (8–10). The TRAP ectodomain contains tandem von Willebrand factor A (VWA) and thrombospondin repeat (TSR) domains. A subset of VWA domains, including the inserted (I) domains in integrins, contain metal ion-dependent adhesion sites (MIDAS), with a Mg^{2+} ion at the center of the ligand binding site (11). Conformational change transmitted from neighboring domains regulates affinity of I domains for ligand. The TRAP VWA domain contains the sequence signature of a MIDAS. Mutations of putative TRAP VWA domain MIDAS residues and deletion of a segment of the TRAP TSR domain disrupt gliding motility and invasion of mosquito salivary glands and mammalian liver cells (12, 13).

A crystal structure of a fragment of the von Willebrand factor A (VWA) domain from a *Toxoplasma gondii* TRAP orthologue, micronemal protein-2 (MIC-2) (5), and an NMR structure of the TRAP TSR domain (4) did not yield insights into conformational regulation or how these neighboring domains might interact in TRAP or MIC-2. In integrins, induction of the high-affinity, open conformation of both the α- and β-subunit I domains is relayed between tandem domains by axial displacement of the C-terminal α helix (14). We hypothesized that the TRAP VWA domain would undergo conformational change during ligand binding, induced by tensile force transmitted through the TSR domain by the motility apparatus. To test this hypothesis, we crystallized TRAP in multiple lattices and conformational states.

Results

A 274-residue *Plasmodium falciparum* TRAP tandem domain fragment (Fig. 1*A*) expressed in mammalian HEK293T cells yielded a 2.2-Å crystal structure of its VWA domain (Table S1 and Fig. S1*A*). The TSR domain was not seen in density, despite its presence in the TRAP construct in crystals as shown by SDS/PAGE (Fig. S1*B*). The C-terminus of the VWA domain lies adjacent to a large void in the crystal lattice (Fig. S1*C*). This void can accommodate multiple orientations of the TSR domain, which must be disordered based on its lack of electron density. A shorter fragment containing the ordered portions of the tandem fragment yielded a second, 2.25-Å, structure (Fig. 1*B* and Table S1). Each of these *P. falciparum* TRAP structures adopts a closed conformation similar to that in integrin I domains. In contrast, a tandem *Plasmodium vivax* TRAP fragment crystallized in a different lattice yielded ordered VWA and TSR domains (Fig. 1*C* and Table S1) with a VWA conformation similar to that in the open conformation of integrin I domains.

The VWA domain is flanked by N-terminal 20-residue and C-terminal 10-residue sequences with one cysteine each that belong by sequence homology to neither the VWA nor TSR domains and are termed here the extensible β ribbon (Fig. 1 *A*–*C*). These segments closely associate with the VWA domain in the closed conformation; indeed, most of the C-terminal segment, including its cysteine, folds up as a portion of the VWA α7 helix and makes α7 longer than in integrin I or VWA domains (Fig. S2). The α7-helix cysteine in the C-terminal extensible β-ribbon segment disulfide bonds to the cysteine in the N-terminal segment. The α7 helix has identical conformations in the two closed structures (Fig. 1 *D* and *E*). The disulfide bond is largely but not completely buried by nearby hydrophobic residues in the VWA α7 helix and central β sheet and by Val-42 in the N-terminal segment. However, most of the N-terminal segment is disordered in the two closed crystal structures. Disordered residues include those that are invariantly conserved as hydrophobic or acidic among diverse *Plasmodium* spp. (Fig. S3). These disordered conserved residues,

Author contributions: G.S. and T.A.S. designed research; G.S. performed research; G.S., A.C.K., C.L., and T.A.S. analyzed data; and G.S. and T.A.S. wrote the paper.

The authors declare no conflict of interest.

Data deposition: Structural data have been deposited in the Protein Data Bank, www.pdb.org (PDB ID codes 4HQF, 4HQK, 4HQO, 4HQL, and 4HQN).

[1]To whom correspondence should be addressed. E-mail: springer@idi.harvard.edu.

This article contains supporting information online at www.pnas.org/lookup/suppl/doi:10.1073/pnas.1218581109/-/DCSupplemental.

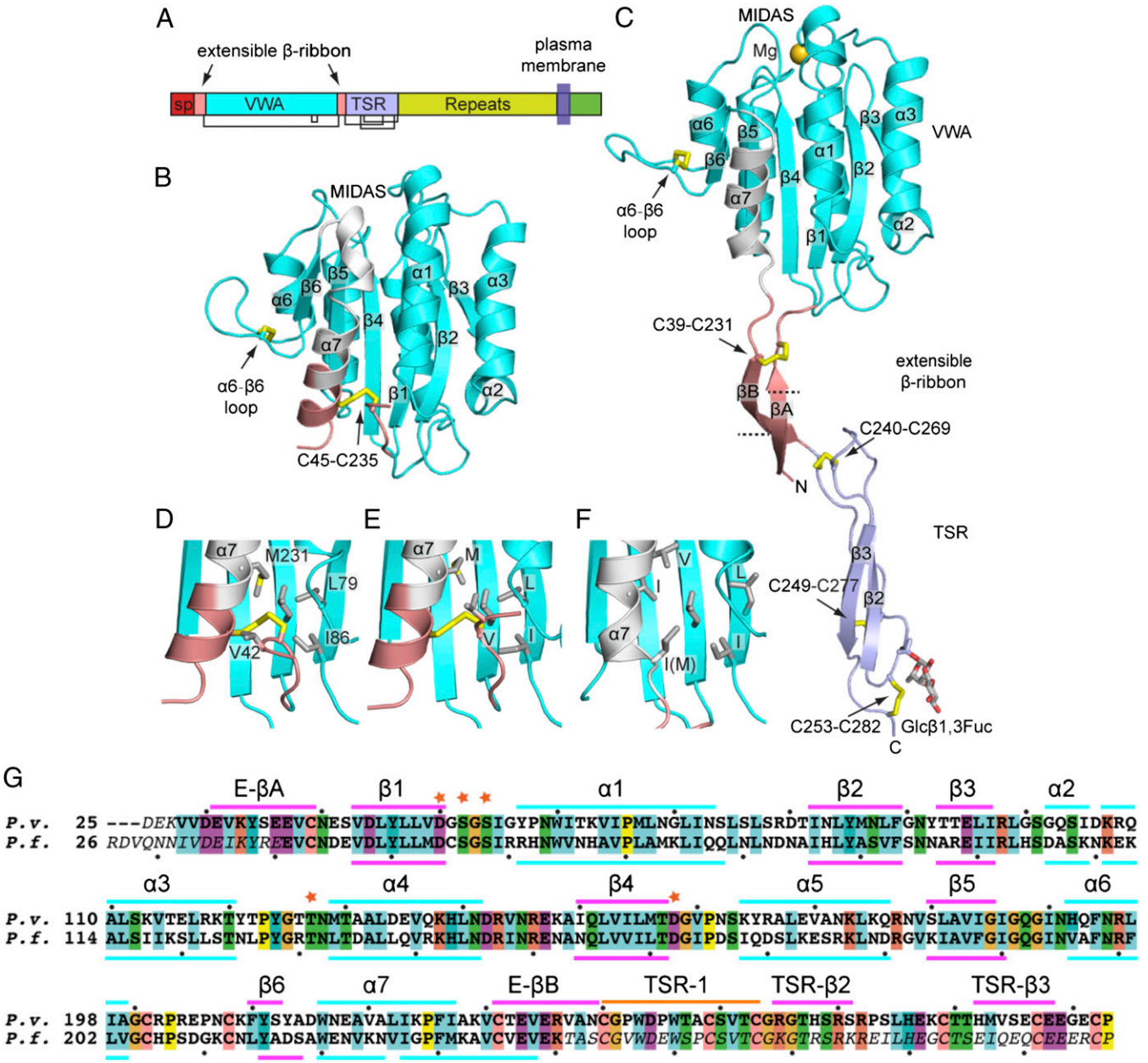

Fig. 1. Structure of TRAP. (*A*) Domain organization, to scale by sequence position. Structure of *P. falciparum* 41-240 fragment (*B*, closed) and *P. vivax* 25-283 fragment (*C*, open) shown in identical orientations. Domains are colored (*B* and *C*) according to the key in (*A*), whereas the VWA β6-α7 loop and α7-helix are white. Disulfide bonds (yellow) and O-linked glycans are shown as sticks. Details near the extensible β ribbon in the closed conformation in *P. falciparum* 26-299 (*D*), *P. falciparum* 41-240 (*E*), and *P. vivax* (*F*) are shown in identical orientations. Sidechains are shown in stick. (*G*) Sequence alignment of *P. vivax* and *P. falciparum* TRAP, with secondary structures in the open and closed conformations shown above and below the alignment, respectively. Disordered residues are italicized. MIDAS residues are asterisked. Dots mark decadal residues.

along with the partial exposure to solvent of hydrophobic residues including the disulfide, may spring-load the extensible β ribbon for conformational change.

A second unique disulfide bond is present within the α6-β6 loop of the VWA domain. The TRAP α6-β6 loop is unusual among VWA domains for its extreme projection from the main body of the domain (Fig. 1 *B* and *C*). The loop folds over a hydrophobic core created by the disulfide bond, toward the putative ligand binding site at the MIDAS of the VWA domain. The disulfide is invariantly conserved in apicomplexan TRAP orthologs including MIC-2 in *T. gondii* (Fig. S3), but was not previously visualized (5).

In the open conformation revealed in the *P. vivax* TRAP crystal structure (Fig. 1*C*), the C-terminal α7 helix of the VWA domain pistons 10 Å in the C-terminal direction compared with the closed conformation and the β6-α7 loop completely reshapes (Figs. 1 *B–F* and 2*A*; the α7-helix and β6-α7 loops are shown in white in Fig. 1 *B–F*). The positions in closed and open conformations of the β6-α7 loop and α7 helices are almost identical between TRAP and integrin αI domains (Fig. 2 *A* and *B*). Furthermore, similar to a Phe in integrins, a Trp in a homologous position of the β6-α7 loop (Fig. S2) is displaced from a hydrophobic pocket in the closed conformation (Fig. 2 *A* and *B*) to make room for new positions of MIDAS loops in the open conformation.

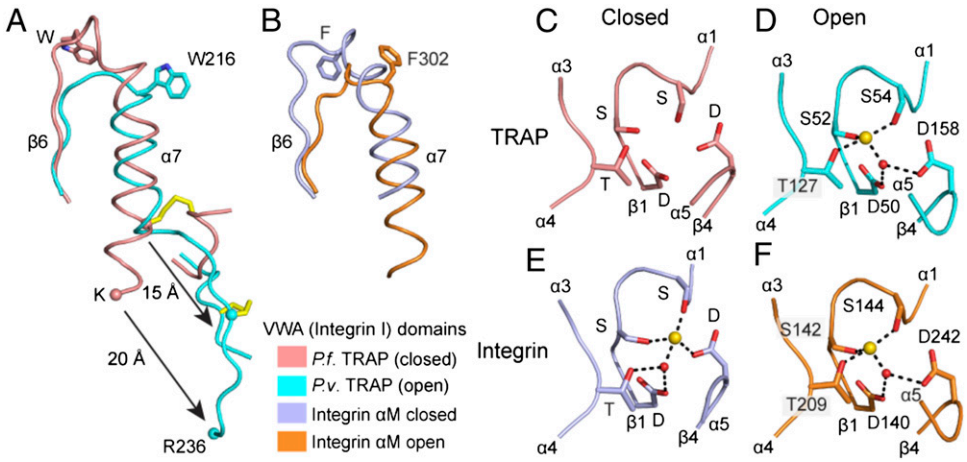

Fig. 2. Conformational change in β6-α7 and MIDAS regions of TRAP VWA and integrin αI domains. The β6-α7 regions in closed and open conformations of TRAP VWA (*A*) and integrin αI (*B*) domains. Fragments are shown in identical orientations after superposition on the entire domain. Homologous Trp and Phe sidechains and the disulfide unique to TRAP are shown in a stick. The last ordered residue in the closed falciparum structure (K240) and its homolog in the open vivax structure (R236) are shown as Cα spheres. (*C–F*) MIDAS structures, with MIDAS residues shown in stick, metal ions as gold spheres, and waters as red spheres. Metal coordinations are dashed. Integrin αM subunit αI domains are from (23).

The MIDAS-coordinating loops of TRAP reorient during conversion from closed to open conformations (Fig. 2 *C* and *D*) and adopt conformations around the MIDAS very similar to those in integrins (Fig. 2 *E* and *F*) (15). From closed to open, the MIDAS α1-β1 loop with its two metal-coordinating Ser residues moves toward a Thr in the α3-α4 loop (Fig. 2 *C–F*). Furthermore, a backbone flip occurs in the β4-α5 loop (Fig. 2 *C–F*). The open TRAP structure has MIDAS loops and a metal ion that are positioned indistinguishably from those in the open conformation of integrin I domains (Fig. 2 *D* and *F*) and quite differently from those in the closed conformation of TRAP VWA or integrin I domains (Fig. 2 *C* and *E*). In the open conformation, the TRAP metal ion has no direct coordinations to negatively charged MIDAS residues, giving it high electrophilicity for negatively charged ligands. Furthermore, rearrangements in MIDAS loops will alter specificity for ligands. Because mutations of the MIDAS-coordinating Thr residue in the TRAP α3-α4 loop and the Asp residue in the β4-α5 loop greatly decrease invasion of mosquito salivary glands and infection of mammalian hosts (12, 13), our structures strongly suggest that conformational change in the VWA domain regulates ligand binding by TRAP during these biological processes.

Extensible β-ribbon formation is coupled to unwinding of the two most C-terminal α-helical turns of the α7 helix (Figs. 1 *B* and *C* and 2*A*). These former α7-helix residues, closely associated N-terminal segment residues, and a total of 13 residues that are disordered in the closed conformation, form a β ribbon composed of two antiparallel β strands that extends 35 Å (Figs. 1*C* and 3 *A–D*).

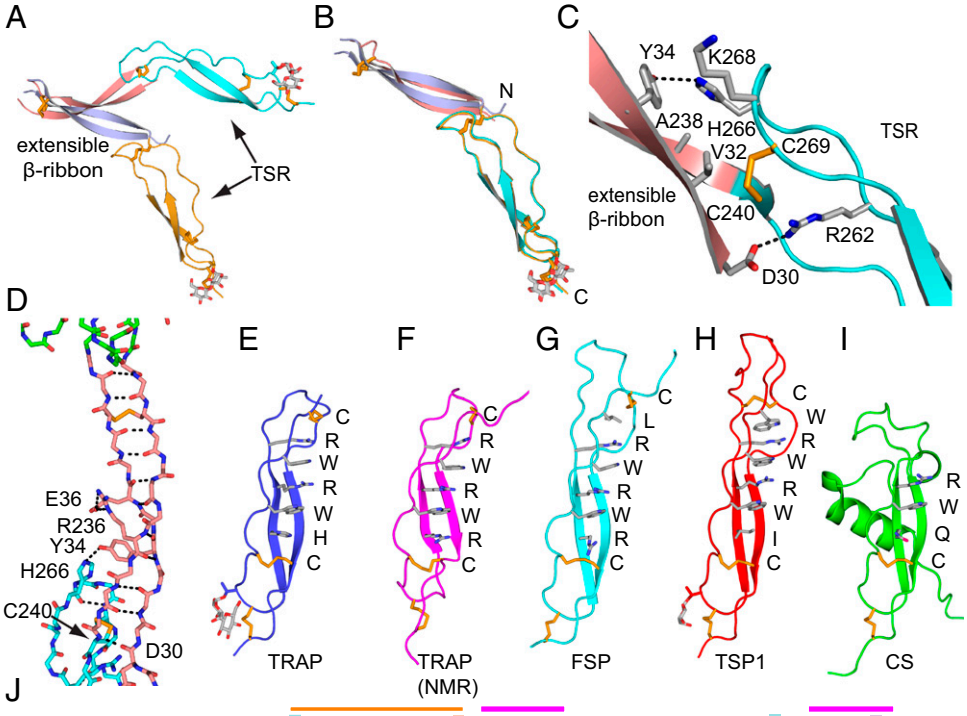

Fig. 3. The extensible β-ribbon and TSR domains. Views of the extensible β ribbon and TSR domain of the two chains in the *P. vivax* open-TRAP structure after superposition on the VWA domain (*A*) or TSR domain (*B*). (*C*) The interface between the extensible β ribbon and TSR domain. Key sidechains are shown as sticks and hydrogen bonds as dashes. (*D*) The backbone of extensible β ribbon with key sidechains and disulfides as sticks, and hydrogen bonds as dashes. (*E–I*) TSR domains. Structures in identical orientations are from our vivax TRAP crystal structure (*E*), an isolated falciparum TRAP TSR domain NMR structure (*F*) (4), and F-spondin (*G*) (48), thrombospondin-1 (*H*) (16), and CS (*I*) (2). Layer residues in TSR domains are shown as sticks and labeled. (*J*) Sequence alignment of representative TSR domains. Cysteines that disulfide link are colored identically. Colored overlines mark strand 1 (orange), β-strands (magenta), and helices (cyan).

Dashed lines on the βA and βB ribbons in Fig. 1*C* mark how far the portions that were in close association with the VWA domain in the closed conformation move in the open conformation. The disulfide bond that stabilizes the α7-helix interface with the N-terminal segment in the closed conformation moves 15 Å and stabilizes the VWA-proximal end of the β ribbon (Figs. 1*C* and 2*A*). The other end of the β ribbon is stabilized by interaction with the TSR domain (Fig. 3 *C* and *D*).

The middle region of the extensible β ribbon is stabilized by a salt bridge between Glu-36 and Arg-236 (Fig. 3*D*), which are invariantly Glu or Arg/Lys in *Plasmodium* spp., respectively (Fig. S3). The sequence of the β ribbon is highly conserved in *Plasmodium* spp. and is rich in β-branched Thr, Val, and Ile residues that favor its β conformation. The length of the β ribbon of 35 Å is very similar to the long dimensions of the VWA and TSR domains. To our knowledge, the appearance through conformational change of an element with domain-like dimensions between two other domains is unprecedented.

TSR domains contain a β ribbon that is augmented by a third "strand" to form the elongated TSR domain (16). Rigidity is provided by closely interacting layers of residues that stack up along one side of the β ribbon (Fig. 3 *E–I*). In the TRAP TSR domain, the layer residues are, from the N-terminal to the C-terminal end, Cys, Arg, Trp, Arg, Trp, His, and Cys (Fig. 3*E*). Differences in the layers at the N-terminal end define four classes of TSR domains, including a highly dissimilar αTSR domain in CS protein (Fig. 3 *E–I*).

Comparisons among two independent, open TRAP molecules in the asymmetric unit show essentially identical orientations between the extensible β ribbon and TSR domain (Fig. 3*B*) that are secured by extensive overlap between the ends of their domains (Fig. 3 *C* and *D*). Such overlap between tandem domains is uncommon, and not seen, for example, between tandem TSR domains in thrombospondin (16). In contrast, orientation between the VWA domain and extensible β-ribbon varies markedly (Fig. 3*A*). The unique specializations at the N-terminal end of the TRAP TSR domain (Fig. 3*E*) stabilize its shape even in isolation (4) (Fig. 3 *E* and *F* and Fig. S4) and create an interface to stabilize the extensible β ribbon once it is formed (Fig. 3*C*). Cys-240 is part of both the extensible β ribbon and TSR domain; as part of the B strand of the β ribbon, it forms the last backbone hydrogen bond of this strand, and as part of the TSR domain, it forms one of its disulfide bonds (Fig. 3 *C* and *D*). This disulfide is in a hydrophobic core at the β-ribbon/TSR overlap with β-ribbon residues Val-32, Tyr-34, and Ala-238 (Fig. 3*C*). His-266 and Lys-268 of TSR help cover the hydrophobic core and form a hydrogen bond and π-cation bond, respectively, to β-ribbon residue Tyr-34. At the opposite end of the overlap, Arg-262 in the second layer position of the TSR salt bridges to Asp-30 of the extensible β ribbon; both residues are invariant in *Plasmodium* spp. (Fig. S3).

The disulfide bond at the C-terminal end of TSR is buried by a glucosyl β1,3-fucose disaccharide. The fucose residue is O-linked to Thr-252 (Figs. 1*C* and 3*E*). Fucosylation is a well-known specialized posttranslational modification of TSR domains (17) but has only occasionally been observed in TSR structures (16). As with TRAP studied here, this modification also occurs in the αTSR domain of CS expressed in mammalian cells (2). It is likely that a similar modification is present on these proteins on the sporozoite surface, because the responsible enzyme in higher eukaryotes, protein O-fucosyl transferase 2, is conserved in *P. falciparum* and other apicomplexans (2).

Discussion

VWA domains are widely expressed intra- and extracellularly in prokaryotes and eukaryotes (11). Only a subset of these have a MIDAS, and fewer still are structurally characterized in two conformational states: integrin αI and βI domains and complement components C2 and factor B (11, 14, 15, 18). Among these, integrin αI domains show the greatest similarity in the mechanism of shape shifting and in being flexibly linked to the domain in which they are inserted in the closed conformation (19). The insertion of the VWA domain in the extensible β-ribbon in TRAP is analogous to insertion of integrin αI and βI domains in β-propeller and hybrid domains, respectively (14, 15). Similarity between TRAP and integrin αI domains may reflect their common function in cell migration and adhesion.

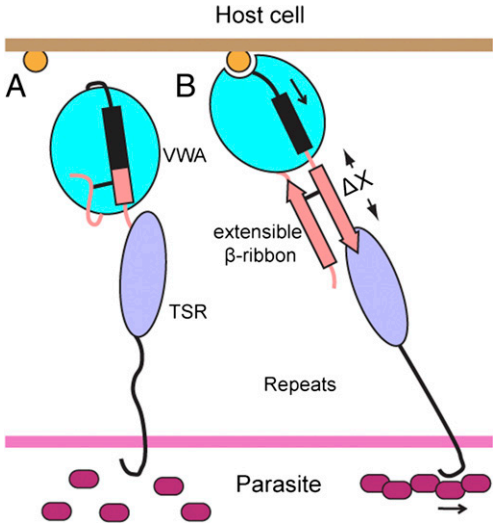

Fig. 4. Model of TRAP activation. (*A*) In the absence of ligand and tensile force, the closed conformation with a flexible orientation between the VWA and TSR domains is favored. (*B*) When an immobilized ligand binds to TRAP through the MIDAS, the tensile force exerted by the parasite actomyosin apparatus will be resisted. TRAP will then be elongated and straightened along the force vector. The elongational force is on pathway with TRAP extension through activation of the VWA domain and formation of the extensible β ribbon. Hence the extended open conformation with putative high-affinity is favored.

We have determined the structure of the majority of the TRAP ectodomain (Fig. 1*A*). The remaining C-terminal segment between the TRAP TSR domain and membrane-spanning domain consists predominantly of proline and polar residues, is likely to be natively unstructured, and to project the ligand-binding domains in TRAP above the protective sheath formed by the CS protein. TRAP has been shown to mediate gliding motility through a "stick-and-slip" process in which different regions of the sporozoite surface alternate between being attached and detached from the substrate (20). Our findings that TRAP exists in both closed and open conformations and that the open, putative high-affinity conformation is linked to TRAP ectodomain extension provides a mechanism for cytoskeletal regulation of stick-and-slip motility.

Tensile force exerted by the parasite actomyosin apparatus on TRAP, when resisted by TRAP binding to a cell or substrate-bound ligand, will elongate and straighten TRAP and align it in the direction of force exertion (Fig. 4). Elongational force will rigidify and thus provide a mechanism for transmitting allostery through the otherwise putatively flexible repeat region. Furthermore, this force is on pathway with and hence energetically favors TRAP extension through formation of the extensible β ribbon and the open, putative high-affinity conformation of the VWA domain (Fig. 4). Because the MIDAS ligand-binding site points in the opposite direction from the C-terminus of the TSR domain (Fig. 4), with a highly elongated domain architecture in between, elongational force is well aligned with protein allostery. Therefore, to a first approximation, the change in free energy of the open conformation relative to the closed conformation of TRAP after application of force can be estimated as $\Delta G = -F\Delta x$.

Knowing that the TSR domain is flexibly connected and is close to the VWA domain in the closed conformation, Δx can be estimated as the length of the extensible β ribbon that is nonoverlapping with the TSR domain, or 25 Å (Fig. 4). This Δx is large compared with other adhesion molecules that exist in flexed, low-affinity, and extended high-affinity states (21). By alternatively engaging and disengaging TRAP localized to different regions of the sporozoite surface with the actomyosin apparatus, stick-and-slip gliding motility may be regulated by force-activated changes in TRAP affinity for ligand (Fig. 4). Cleavage in the TRAP transmembrane domain by a rhomboid protease is also required for sporozoite motility (22). Thus, cleavage of TRAP that is engaged by extracellular ligand and the sporozoite motility apparatus may be another important mechanism of detachment at the posterior end of the sporozoite that enables new sites of attachment at the anterior end to provide traction for continued motility.

It is fortuitous that two conformational states, open and closed, were glimpsed here with TRAP from different species. The TRAPs from *P. vivax* and *P. falciparum* are orthologues and their VWA, extensible β-ribbon, and TSR domains are 49% identical in sequence overall. Current knowledge about protein structure and function, as well as what we know about integrins, teaches us that at this level of sequence identity, TRAP from all species of Plasmodia, as well as orthologues in other genera such as MIC2 in Toxoplasma, must also have closed and open conformational states. Interestingly, the αI domain of integrin αMβ2 also has been crystallized in open and closed conformations, depending on the crystal lattice (23).

TRAP supports sporozoite gliding motility in remarkably varied host environments, and also in vitro on artificial substrates (6). In the mosquito, TRAP is required for migration from the hemolymph into salivary glands. In vertebrates, TRAP is required for emigration from the dermis into blood vessels, and from blood vessels into liver (12, 13). In the liver, sporozoites must enter the space of Disse, possibly through Kupffer cells (24), before traversing through a few hepatocytes before invading one (25). Furthermore, TRAP supports two different types of behavior. In cell traversal, the plasma membrane is wounded on either side of a cell as a sporozoite passes through. In invasion, a moving junction containing TRAP is formed between the parasite and hepatocyte plasma membranes as the parasitophorous vacuole is formed around the sporozoite (6, 24, 25). Thus far, understanding of the ligands encountered by the sporozoite on its long journey is meager, but the list includes heparin (24, 26–28). Our ability to produce well-folded TRAP and characterize a putative high affinity state promises to further advance ligand identification. Several other sporozoite microneme proteins that have VWA and/or TSR domains also contribute to the sporozoite journey; however, thus far, mutational studies suggest that TRAP is by far the most important (6, 12, 13, 29, 30).

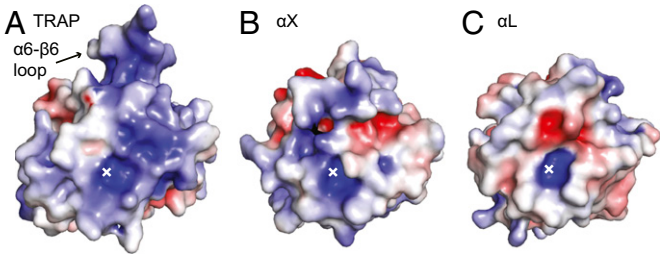

Fig. 5. Electrostatics of TRAP and integrin αI domains. Surfaces of open vivax TRAP VWA (*A*) and integrin αI domains (*B* and *C*) are shown in identical orientations, with the position of the MIDAS metal ion marked with an x. Electrostatic solvent accessible surfaces [−5 (red) to +5 (blue) kT/e] were calculated using the Poisson–Boltzmann approximation.

The overall shape and charge of the ligand-binding surface surrounding the MIDAS are distinctive in TRAP. In TRAP, the area surrounding the MIDAS is flatter than in integrin αI domains, and when viewed normal to this flat surface, the surrounding area is larger (Fig. 5). These differences hold up whether TRAP is compared with integrin α2, αL, αM, or αX αI domains. It is possible that this large, flat surface surrounding the MIDAS is a specialization for binding a large number of ligands with high affinity. The unique shape of this surface in TRAP compared with integrin αI domains is constructed from TRAP's unique disulfide-bonded α6-β6 loop, differences in the β4-α5 and β5-α6 loops, and longer α5 and shorter α6 helices in TRAP.

The high isoelectric point (pI) of TRAP may also be important for ligand binding. TRAP VWA domains are basic, with estimated pI values in the range of 9 to 10. In contrast, the majority of proteins are acidic with a pI between 5 and 6. Furthermore, cell surfaces are negatively charged and heparan sulfate-proteoglycans are highly negatively charged. The unusually high sulfation of heparan sulfate in the liver sets it apart from other tissues and may contribute to targeting sporozoites to the liver (24). Positively charged surfaces on TRAP that are candidates for heparin binding include the region around the MIDAS, and two crevices that are formed on either side of the unique α6-β6 loop that projects from the body of the VWA domain (Fig. 5a).

In its likely ability to bind multiple ligands, TRAP is reminiscent of integrins αXβ2 and αMβ2. These integrins bind a wide variety of ligands that include the complement opsonic fragment iC3b, intercellular adhesion molecule-1, heparin, and denatured proteins. An acidic group is key in ligands (refs. 31–33 and references therein). Interestingly, the promiscuous, heparin-binding integrin αI domains of αXβ2 (Fig. 5*B*) and αMβ2 (31, 33) have higher pI values in the range of 9 to 10 than those of the more selective αLβ2 (pI 6, Fig. 5*C*) or α2β1 (pI 8) integrins.

Our ability to express, purify, and conformationally characterize all structured modules in TRAP is a marked advance toward subunit malaria vaccines. The anti-sporozoite subunit vaccine currently in clinical trials, RTS,S, contains a CS protein fragment, and gives limited protection (34). TRAP has shown efficacy in animal models with tumor cell transfectants coexpressing TRAP and CS (35) and in virally vectored prime and boost vaccines (36). These vaccines express apicomplexan sequences in mammalian hosts. Our constructs remove one (*P. falciparum*) or four (*P. vivax*) *N*-glycosylation sites that, when not mutated, are *N*-glycosylated in mammalian expression hosts (Fig. S5). In a subunit vaccine trial, immunization of rhesus infants and adults with RTS,S together with TRAP expressed in insect cells revealed antibody responses to TRAP and better T-cell responses to TRAP than to RTS,S, especially in infants (37). However, the sequence of the TRAP fragment that was used, its characterization, or whether it was expressed in the cytoplasm, on the cell surface, or secreted by insect cells, was not disclosed. Thus, it is difficult to know whether TRAP used previously was *N*-glycosylated, had proper disulfide linkages, and was fully folded.

Whether sporozoite proteins are N-glycosylated is an important question. Only recently, Plasmodial species have been shown to contain the genes for constructing lipid-linked, unusually short, $GlcNAc_2$ N-glycan precursors and transferring them to proteins. Furthermore, the presence of dolichol-phosphate linked GlcNAc and $GlcNAc_2$ precursors, and $GlcNAc_2$-bearing proteins, was demonstrated in *P. falciparum* erythroid forms (38). It will be interesting to determine whether TRAP and other sporozoite stage surface proteins also bear these unusually truncated N-glycans. A potential *N*-glycosylated Asn residue immediately follows MIDAS residue Thr-131 (*P. falciparum*) and Thr-127 (*P. vivax*) (Fig. 1*G*). Differences in *N*-linked glycosylation between *Plasmodium* and higher eukaryotes thus could have a major impact on recognition of the MIDAS region by function-blocking antibodies and will be an important consideration for subunit vaccines.

Structural vaccinology of influenza and HIV has shown that important epitopes may only be exposed after initial contact with host cells (39–41); the open conformation of TRAP may be analogous. Whether antibodies to the closed TRAP conformation or to its open conformation with its β ribbon extended will be more protective is currently unknown. The current work establishes the foundation for definitive testing of whether a subunit vaccine containing TRAP, either in a mixture of conformational states, mutationally stabilized in one state, or in combination with CS, can be efficacious for preventing infection by falciparum or vivax species of malaria.

Materials and Methods

Synthetic cDNA sequences optimized for mammalian expression for TRAP residues 26-299 or 41-240 with C55G and N132S mutations (*P. falciparum*, GenBank accession no. AAA29775) or residues 25-283 with S42Q, N91S, N128S, and S180R mutations (*P. vivax*, GenBank accession no. AAC97484) to remove a nonconserved Cys or *N*-linked sites were inserted between murine Ig chain signal peptide and HHHHHHA sequences in plasmid pLEXm (42). HEK293T cells were transiently transfected using polyethylenimine (43). Culture supernatants (1 L) were harvested after 5 d. Purification was with Ni-NTA affinity (43) followed by Superdex S200 gel filtration in 20 mM Hepes 7.2 and 300 mM NaCl. Purified protein was concentrated to 5 mg/mL (*P. falciparum*) or 7.5 mg/mL (*P. vivax*) and stored at −80 °C. Diffraction-quality *P. falciparum* 26-299 TRAP crystals were produced at 4 °C in 0.1 M Tris 8.5, 0.2 M Li_2SO_4, and 25% PEG 4000. Single crystals were directly frozen in liquid nitrogen. *P. falciparum* 41-240 TRAP crystallized at 20 °C in 0.1 M Hepes 7.5, 2% PEG 400, and 2 M $(NH_4)_2SO_4$. Crystals were transferred to mother liquor supplemented with 25% glycerol, then frozen in liquid nitrogen. *P. vivax* TRAP crystallized with 15% PEG 20000 and 0.1 M Tris 8.5 at 4 °C. Crystals were transferred to mother liquor supplemented with 20% glycerol in 5% steps, then frozen in liquid nitrogen. Density for Mg^{2+} was present at the MIDAS in chain A, despite absence from buffers. Further crystals soaked in mother liquor supplemented with 5 mM Mg^{2+} or 2 mM Mn^{2+} showed strong metal density at the MIDAS in both chains A and B.

Diffraction data were collected at 100 K. The data were indexed and scaled with HKL2000. Structures were solved by molecular replacement using VWA domain (PDB ID 1shu) as a search model with MolREP (44). Model rebuilding and refinement were with Coot (45) and PHENIX (46). Model validation was with MOLPROBITY (47).

ACKNOWLEDGMENTS. We thank Jianghai Zhu for help with structure solution and model building. We thank the staff at the General Medical Sciences and Cancer Institutes Structural Biology Facility (GM/CA) beamline 23-ID at Advanced Photon Source (Argonne, IL) for data collection support. This work was supported by National Institutes of Health Grant AI095686.

1. Plassmeyer ML, et al. (2009) Structure of the *Plasmodium falciparum* circumsporozoite protein, a leading malaria vaccine candidate. *J Biol Chem* 284(39):26951–26963.
2. Doud MB, et al. (2012) An unexpected fold in the circumsporozoite protein target of malaria vaccines. *Proc Natl Acad Sci USA* 109(20):7817–7822.
3. Coppi A, et al. (2011) The malaria circumsporozoite protein has two functional domains, each with distinct roles as sporozoites journey from mosquito to mammalian host. *J Exp Med* 208(2):341–356.
4. Tossavainen H, et al. (2006) The layered fold of the TSR domain of *P. falciparum* TRAP contains a heparin binding site. *Protein Sci* 15(7):1760–1768.
5. Tonkin ML, Grujic O, Pearce M, Crawford J, Boulanger MJ (2010) Structure of the micronemal protein 2 A/I domain from *Toxoplasma gondii*. *Protein Sci* 19(10):1985–1990.
6. Kappe SH, Buscaglia CA, Nussenzweig V (2004) Plasmodium sporozoite molecular cell biology. *Annu Rev Cell Dev Biol* 20:29–59.
7. Rogers WO, et al. (1992) Characterization of *Plasmodium falciparum* sporozoite surface protein 2. *Proc Natl Acad Sci USA* 89(19):9176–9180.
8. Kappe S, et al. (1999) Conservation of a gliding motility and cell invasion machinery in Apicomplexan parasites. *J Cell Biol* 147(5):937–944.
9. Jewett TJ, Sibley LD (2003) Aldolase forms a bridge between cell surface adhesins and the actin cytoskeleton in apicomplexan parasites. *Mol Cell* 11(4):885–894.
10. Buscaglia CA, Coppens I, Hol WG, Nussenzweig V (2003) Sites of interaction between aldolase and thrombospondin-related anonymous protein in plasmodium. *Mol Biol Cell* 14(12):4947–4957.
11. Springer TA (2006) Complement and the multifaceted functions of VWA and integrin I domains. *Structure* 14:1611–1616.
12. Wengelnik K, et al. (1999) The A-domain and the thrombospondin-related motif of *Plasmodium falciparum* TRAP are implicated in the invasion process of mosquito salivary glands. *EMBO J* 18(19):5195–5204.
13. Matuschewski K, Nunes AC, Nussenzweig V, Menard R (2002) Plasmodium sporozoite invasion into insect and mammalian cells is directed by the same dual binding system. *EMBO J* 21(7):1597–1606.
14. Springer TA, Dustin ML (2012) Integrin inside-out signaling and the immunological synapse. *Curr Opin Cell Biol* 24(1):107–115.
15. Shimaoka M, Takagi J, Springer TA (2002) Conformational regulation of integrin structure and function. *Annu Rev Biophys Biomol Struct* 31:485–516.
16. Tan K, et al. (2002) Crystal structure of the TSP-1 type 1 repeats: a novel layered fold and its biological implication. *J Cell Biol* 159(2):373–382.
17. Hofsteenge J, et al. (2001) C-mannosylation and O-fucosylation of the thrombospondin type 1 module. *J Biol Chem* 276:6485–6498.
18. Forneris F, et al. (2010) Structures of C3b in complex with factors B and D give insight into complement convertase formation. *Science* 330(6012):1816–1820.
19. Xie C, et al. (2010) Structure of an integrin with an α I domain, complement receptor type 4. *EMBO J* 29(3):666–679.
20. Munter S, et al. (2009) Plasmodium sporozoite motility is modulated by the turnover of discrete adhesion sites. *Cell Host Microbe* 6(6):551–562.
21. Astrof NS, Salas A, Shimaoka M, Chen JF, Springer TA (2006) Importance of force linkage in mechanochemistry of adhesion receptors. *Biochemistry* 45:15020–15028.
22. Ejigiri I, et al. (2012) Shedding of TRAP by a rhomboid protease from the malaria sporozoite surface is essential for gliding motility and sporozoite infectivity. *PLoS Pathog* 8(7):e1002725.
23. Lee J-O, Bankston LA, Arnaout MA, Liddington RC (1995) Two conformations of the integrin A-domain (I-domain): a pathway for activation? *Structure* 3:1333–1340.
24. Pradel G, Garapaty S, Frevert U (2004) Kupffer and stellate cell proteoglycans mediate malaria sporozoite targeting to the liver. *Comp Hepatol* 3(Suppl 1):S47.
25. Mota MM, et al. (2001) Migration of *Plasmodium* sporozoites through cells before infection. *Science* 291(5501):141–144.
26. Ghosh AK, et al. (2009) Malaria parasite invasion of the mosquito salivary gland requires interaction between the *Plasmodium* TRAP and the Anopheles saglin proteins. *PLoS Pathog* 5:e1000265.
27. McCormick CJ, Tuckwell DS, Crisanti A, Humphries MJ, Hollingdale MR (1999) Identification of heparin as a ligand for the A-domain of *Plasmodium falciparum* thrombospondin-related adhesion protein. *Mol Biochem Parasitol* 100(1):111–124.
28. Jethwaney D, et al. (2005) Fetuin-A, a hepatocyte-specific protein that binds *Plasmodium berghei* thrombospondin-related adhesive protein: a potential role in infectivity. *Infect Immun* 73(9):5883–5891.
29. Moreira CK, et al. (2008) The *Plasmodium* TRAP/MIC2 family member, TRAP-Like Protein (TLP), is involved in tissue traversal by sporozoites. *Cell Microbiol* 10(7):1505–1516.
30. Hegge S, et al. (2010) Multistep adhesion of *Plasmodium* sporozoites. *Faseb J* 24(7):2222–2234.
31. Diamond MS, Alon R, Parkos CA, Quinn MT, Springer TA (1995) Heparin is an adhesive ligand for the leukocyte integrin Mac-1 (CD11b/CD18). *J Cell Biol* 130(6):14731482.
32. Vorup-Jensen T, et al. (2005) Exposure of acidic residues as a danger signal for recognition of fibrinogen and other macromolecules by integrin $\alpha_X\beta_2$. *Proc Natl Acad Sci USA* 102(5):1614–1619.
33. Vorup-Jensen T, et al. (2007) Binding between the integrin $\alpha_X\beta_2$ (CD11c/CD18) and heparin. *J Biol Chem* 282:30869–30877.
34. Agnandji ST, et al. (2011) First results of phase 3 trial of RTS, S/AS01 malaria vaccine in African children. *N Engl J Med* 365(20):1863–1875.
35. Khusmith S, et al. (1991) Protection against malaria by vaccination with sporozoite surface protein 2 plus CS protein. *Science* 252(5006):715–718.
36. Hill AV, et al. (2010) Prime-boost vectored malaria vaccines: progress andprospects. *Hum Vaccin* 6(1):78–83.
37. Walsh DS, et al. (2004) Safety and immunogenicity of RTS,S+TRAP malaria vaccine, formulated in the AS02A adjuvant system, in infant rhesus monkeys. *Am J Trop Med Hyg* 70(5):499–509.
38. Bushkin GG, et al. (2010) Suggestive evidence for Darwinian Selection against asparagine-linked glycans of *Plasmodium falciparum* and *Toxoplasma gondii*. *Eukaryot Cell* 9(2):228–241.
39. Harrison SC (2008) Viral membrane fusion. *Nat Struct Mol Biol* 15(7):690–698.
40. Thali M, et al. (1993) Characterization of conserved human immunodeficiency virus type 1 gp120 neutralization epitopes exposed upon gp120-CD4 binding. *J Virol* 67(7):3978–3988.
41. Xiang SH, Doka N, Choudhary RK, Sodroski J, Robinson JE (2002) Characterization of CD4-induced epitopes on the HIV type 1 gp120 envelope glycoprotein recognized by neutralizing human monoclonal antibodies. *AIDS Res Hum Retroviruses* 18(16):1207–1217.
42. Aricescu AR, Lu W, Jones EY (2006) A time- and cost-efficient system for high level protein production in mammalian cells. *Acta Crystallogr D Biol Crystallogr* 62(Pt 10):1243–1250.
43. Zhou Y, et al. (2011) A pH-regulated dimeric bouquet in the structure of von Willebrand factor. *EMBO J* 30(19):4098–4111.
44. Vagin A, Teplyakov A (2010) Molecular replacement with MOLREP. *Acta Crystallogr D Biol Crystallogr* 66(Pt 1):22–25.
45. Emsley P, Cowtan K (2004) Coot: model-building tools for molecular graphics. *Acta Crystallogr D Biol Crystallogr* 60:2126–2132.
46. Adams PD, et al. (2010) PHENIX: a comprehensive Python-based system for macromolecular structure solution. *Acta Crystallogr D Biol Crystallogr* 66(Pt 2):213–221.
47. Davis IW, et al. (2007) MolProbity: all-atom contacts and structure validation for proteins and nucleic acids. *Nucleic Acids Res.* 35:W375–W383.
48. Paakkonen K, et al. (2006) Solution structures of the first and fourth TSR domains of F-spondin. *Proteins* 64(3):665–672.

Supporting Information

Song et al. 10.1073/pnas.1218581109

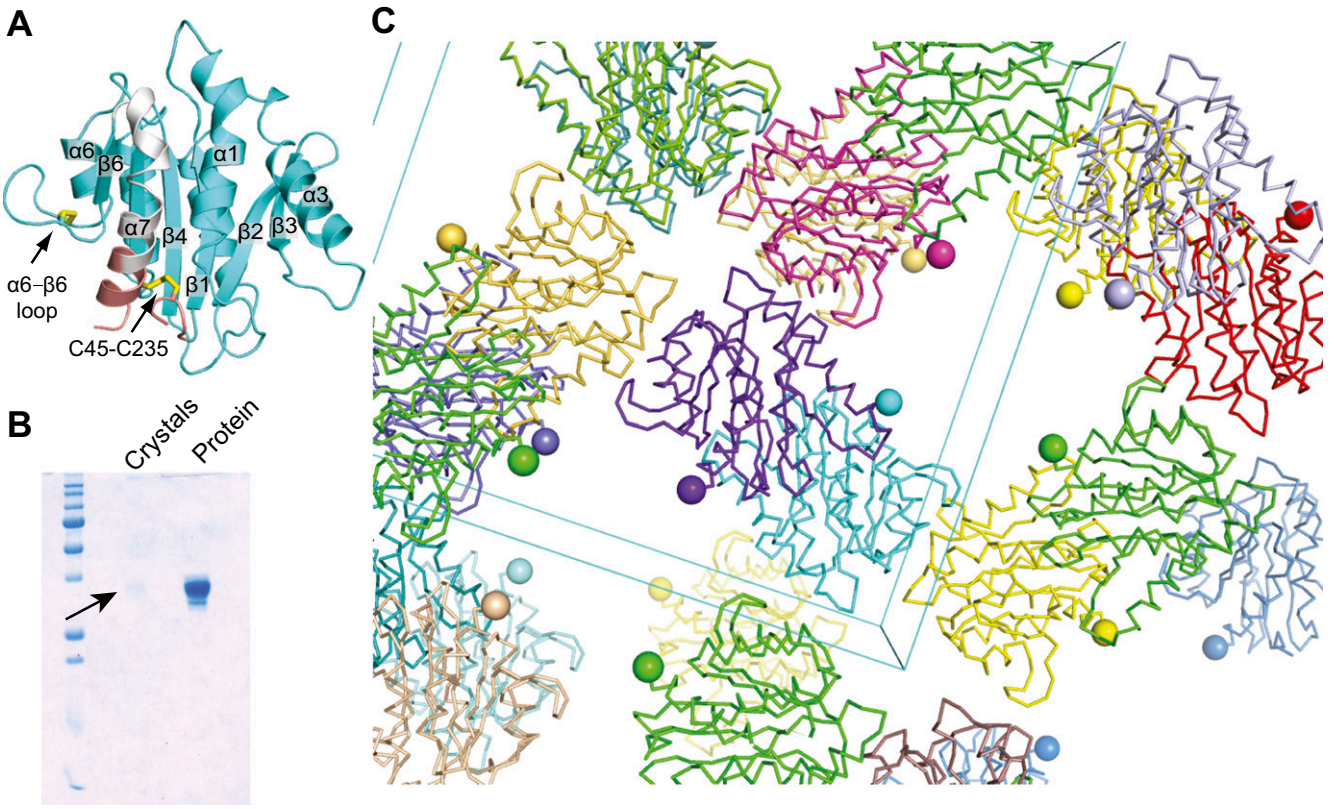

Fig. S1. TSR domain is present in pfTRAP (26-299) crystals, but missing in electron density. (*A*) The structure of pfTRAP (26–299) VWA domain in the same orientation as in Fig. 1 *B* and *C*. (*B*) SDS/PAGE of dissolved crystals and the TRAP protein that was subjected to crystallization. (*C*) Packing of pfTRAP (26–299) VWA domain in crystal lattice. The chains are shown as ribbons and the Cα of terminal residues K240 are shown as spheres.

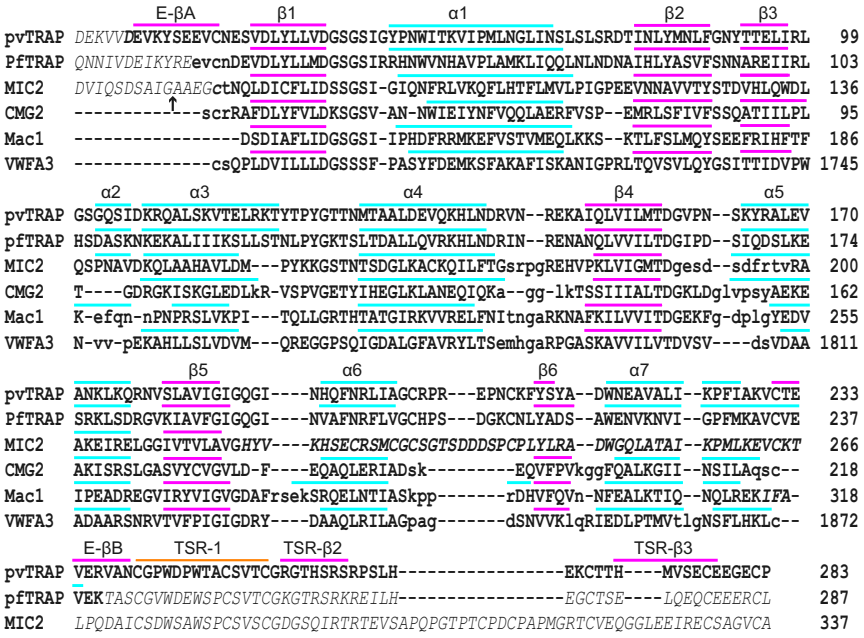

Fig. S2. Structure-based alignment of TRAP with representative VWA domains. VWA domain structures were aligned using secondary-structure matching (1). Some gaps were closed up manually; resulting structurally nonequivalent aligned residues are in lowercase. Residues not present in crystallized proteins or missing in density are in italics. Aligned structures are MIC (2), CMG2 (3), Mac-1 (4), and VWF A3 (5). The MPP2 cleavage site in MIC2 is indicated by an arrow.

1. Krissinel E, Henrick K (2004) Secondary-structure matching (SSM), a new tool for fast protein structure alignment in three dimensions. *Acta Crystallogr D Biol Crystallogr* 60(Pt 12 Pt 1): 2256–2268.
2. Tonkin ML, Grujic O, Pearce M, Crawford J, Boulanger MJ (2010) Structure of the micronemal protein 2 A/I domain from Toxoplasma gondii. *Protein Sci* 19(10):1985–1990.
3. Lacy DB, Wigelsworth DJ, Scobie HM, Young JA, Collier RJ (2004) Crystal structure of the von Willebrand factor A domain of human capillary morphogenesis protein 2: An anthrax toxin receptor. *Proc Natl Acad Sci USA* 101(17):6367–6372.
4. Lee JO, Rieu P, Arnaout MA, Liddington R (1995) Crystal structure of the A domain from the α subunit of integrin CR3 (CD11b/CD18). *Cell* 80(4):631–638.
5. Bienkowska J, Cruz M, Atiemo A, Handin R, Liddington R (1997) The von willebrand factor A3 domain does not contain a metal ion-dependent adhesion site motif. *J Biol Chem* 272(40): 25162–25167.

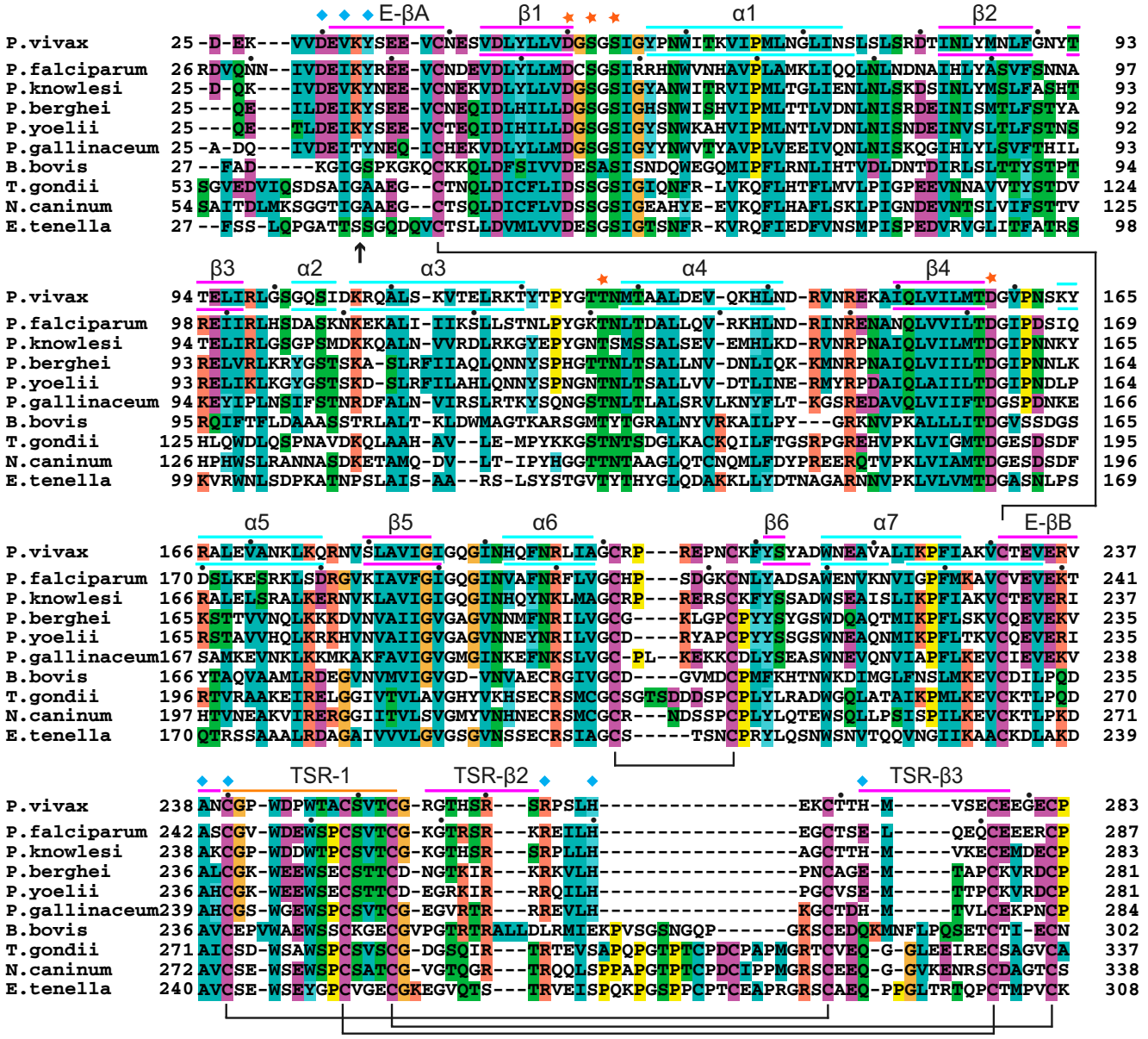

Fig. S3. Sequence alignment of the N-terminal TRAP segment containing the VWA and TSR domains with orthologs in other apicomplexan species. Sequences have GenBank accession numbers AAC97484 (*P. vivax*), AAA29775 (*P. falciparum*), AAG24613 (*Plasmodium knowlesi*), AAB63302 (*Plasmodium berghei*), AAA29768 (*Plasmodium yoelii*), AAC47461 (*Plasmodium gallinaceum*), ACM44016 (*Babesia bovis*), AAB63303 (*Toxoplasma gondii*), AAF01565 (*Neospora caninum*), and AAD03350 (*Eimeria tenella*). Secondary structures are marked above the sequences of *P. vivax* and *P. falciparum* TRAP constructs. MIDAS residues are marked with asterisks. Disulfide-bonded residues are linked by black lines for *P. vivax* and *P. falciparum*. Conserved residues within the interface between the extensible β ribbon and TSR domain are marked with blue diamonds. Black dots mark decadal residues. In MIC2, E-βA differs. The long loop between TSR-β2 and TSR-β3 in MIC2 with its additional two cysteines is predicted to extend the interaction interface between the TSR domain and extensible β ribbon and compensate for the different character of extensible β ribbon E-βA in MIC2.

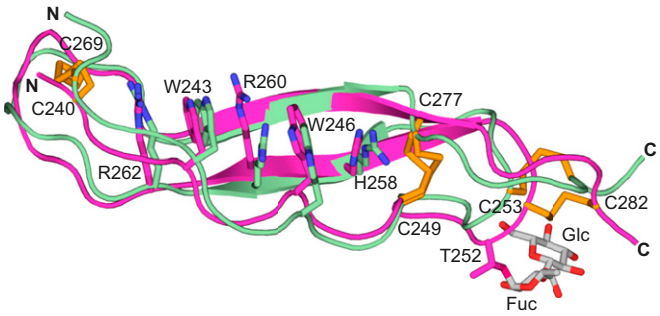

Fig. S4. Superposition of TRAP TSR domains from *P. vivax* crystal structure and *P. falciparum* NMR structures. Backbones are magenta for *P. vivax* and green for *P. falciparum* (model 1 of PDB ID 2BBX). The TSR layer residues and the carbohydrate (present only in the crystal structure) are shown as sticks. Residue numbering is for *P. vivax*; His258 is Arg in *P. falciparum*.

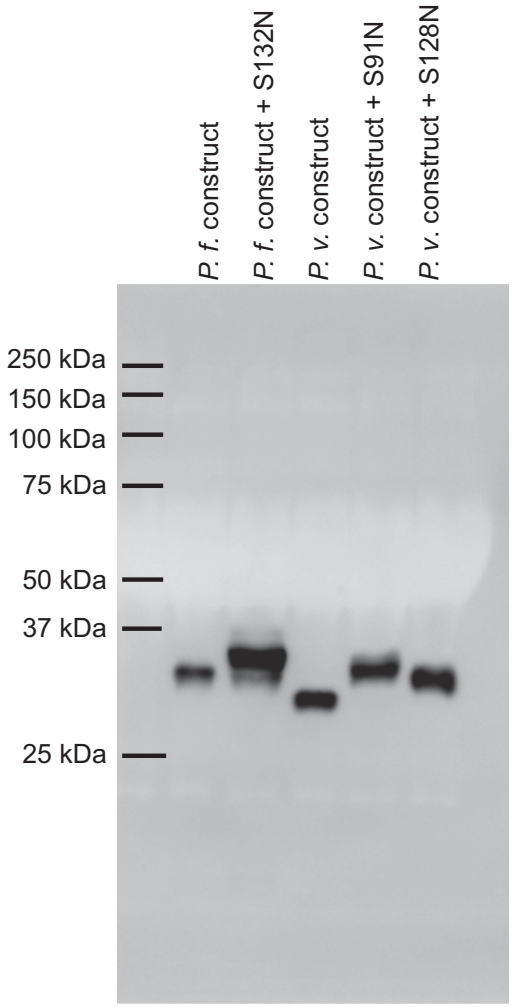

Fig. S5. *N*-glycosylation of back-mutated constructs in 293T cells. The crystallization constructs with all potential *N*-linked sites mutated and indicated back-mutations to wild-type sequence are compared. Culture supernatants from transient transfections were subjected to reducing SDS 12.5% PAGE and anti-His Western blotting.

Table S1. Data collection and refinement statistics

	pfTRAP (26-299)	pfTRAP (41-240)	pvTRAP	pvTRAP (Mg)	pvTRAP (Mn)
Data					
Space group	I4	$P42_12$	$P2_12_12_1$	$P2_12_12_1$	$P2_12_12_1$
Cell dimensions					
a, *b*, *c* (Å)	110.2, 110.2, 47.0	117.7, 117.7, 65.5	56.3, 100.5, 158.6	59.6, 98.0, 159.2	59.6, 98.6,159.5
α, β, γ (°)	90, 90, 90	90, 90, 90	90, 90, 90	90, 90, 90	90, 90, 90
Resolution (Å)	43.27–2.2 (2.26–2.2)	41.03–2.25 (2.29–2.25)	42.43–2.2 (2.24–2.2)	41.72–2.24 (2.28–2.24)	39.88–2.2 (2.24–2.2)
R_{sym}*	0.165 (1.123)	0.157 (1.000)	0.071 (0.315)	0.085 (0.353)	0.132 (0.948)
I/σI	11.26 (1.69)	10.22 (1.28)	16.72 (3.69)	13.73 (4.36)	10.61 (1.49)
Completeness (%)	98.1 (97.5)	99.9 (99.6)	98.3 (88.0)	99.6 (99.1)	99.7 (99.4)
Redundancy	2.89 (2.80)	6.8 (5.7)	3.8 (3.5)	4.0 (3.8)	4.0 (3.8)
Refinement					
Resolution (Å)	43.27–2.2	41.03–2.25	42.43–2.2	41.72–2.24	39.88–2.2
No. reflections	14,268	22,394	46,091	45,385	47,461
R_{work}/R_{free}†	0.17/0.22	0.19/0.24	0.16/0.20	0.16/0.20	0.17/0.21
rms deviations					
Bond lengths (Å)	0.008	0.003	0.009	0.008	0.007
Bond angles (°)	1.10	0.70	0.99	1.00	0.99
Residue range	41–240	41–240	25–283	28–283	28–283
Ramachandran (%)‡	98.0/2.0/0	96.7/3.3/0	96.3/3.7/0	97.4/2.6/0	96.1/3.9/0
PDB code	4HQF	4HQK	4HQO	4HQL	4HQN

Values for highest resolution shells are in parentheses.

*$R_{sym} = \Sigma i,h|I(i,h) - <I(h)>|/\Sigma i,h|I(i,h)|$ where $I(i,h)$ and $<I(h)>$ are the ith and mean measurement of intensity of reflection h.

†R_{free} was calculated using 5% of the data.

‡Residues in favored, accepted, and outlier regions of the Ramachandran plot as reported by MOLPROBITY.